The Effect of Access Port Placement on the Tritium Breeding Ratio in an EU DEMO Tokamak

J.H. Bernardi (St John's College Cambridge), Dr. J. Shimwell (CCFE, Oxon)
CCFE, Culham Science Centre, Abingdon, Oxon, OX14 3DB, UK
Bernardi.James.H@gmail.com

Abstract

Neutronics simulations were carried out on multiple models of the European Union Demonstration Power Plant (EU DEMO). These models were generated automatically with differing access port placement to investigate the placement's effect on the tritium breeding ratio (TBR). In doing so, a study was made into the extent to which neutrons' interactions (such as reflection) between ports have a meaningful effect on the TBR, or how far the TBR depends purely on the amount of the front-facing surface area of reactor blanket available. This study found that the specific arrangement of access ports between models with up to 16 ports did not affect the TBR value by more than 0.01, and some differences corresponded with blanket surface area remaining. Despite the small differences in TBR, some patterns began to emerge, potentially showing favour towards a small lateral angle off the equator, which may be explained by a smaller amount of surface area lost when placing ports in these positions. This study concludes with potential directions in which future, more computationally expensive tests could probe to make further conclusions.

1 - Introduction

1.1 Context and Background

The European Union Demonstration Power Plant (EU DEMO) has the ultimate goal of producing sustained electricity to a grid by accessing the energy released by Deuterium-Tritium (D-T) fusion:

$$ {}^{2}_{1}H + {}^{3}_{1}H \rightarrow {}^{4}_{2}He + {}^{1}_{0}n + 17.59\,MeV. \quad \text{(eq. 1)} $$

To do so, it must have a sustained supply of fuel. Extraction of deuterium (${}^{2}_{1}H$) from seawater is a well-known industrial process, however there is currently no known method of obtaining tritium (${}^{3}_{1}H$) off-site, at least in quantities viable for fuelling sustained nuclear fusion. This is in part due to its short half life of around 12 years, thus scarcity in nature.

For these reasons, all the fuel for a reactor (and start-up fuel for any newly built reactors: see 'reactor doubling time') must be bred in-situ. The expelled 14.1MeV neutron (in equation 1) escapes the plasma-confining magnetic field (as it is neutral), and is utilised in the 'blanket structure' surrounding the fusion chamber to produce tritium fuel. This section will continue to explain the mechanisms by which this takes place. Figure 2.1.1 provides a basic visualisation of the structure referenced throughout this section, if required.

The first process this blanket structure is accountable for is direct tritium breeding. This is achieved with the expelled neutron via the following reactions with lithium:

$$ {}^{6}_{3}Li + {}^{1}_{0}n \rightarrow {}^{4}_{2}He + {}^{3}_{1}H + 4.8MeV, \quad \text{(eq. 2)} $$

$$ {}^{7}_{3}Li + {}^{1}_{0}n \rightarrow {}^{3}_{2}He + {}^{3}_{1}H + {}^{1}_{0}n - 2.5MeV. \quad \text{(eq. 3)} $$

Figures 1.1.1 and 1.1.2 depict the evolution of the expelled-neutron spectrum, with figure 1.1.1 representing the relative spectrum at the 'first wall'- a structure protecting the tritium breeding blanket- and figure 1.1.2 is the relative spectrum outside the blanket structure- the 'vacuum vessel'.

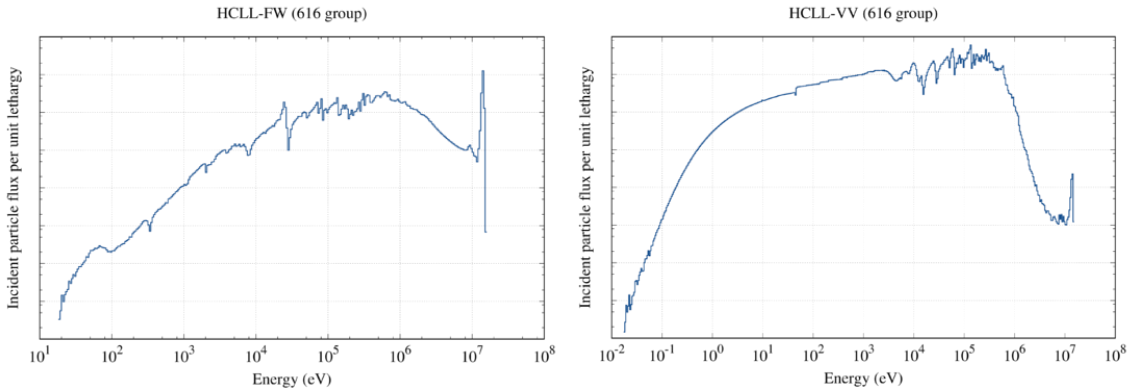

Fig 1.1.1, 1.1.2 (left, right): Reference Input Neutron Spectra for 'Helium Cooled Lithium-Lead' (HCLL) in the 'First Wall' (FW- protects the blanket) and 'Vacuum Vessel' (VV- a void between the blanket material and the back-support-structure, e.g. after the wall). Data taken from the FISPACT-II Wiki.

The differences in the above neutron spectra are accounted for by considering scattering interactions throughout the blanket. Neutrons in this lithium-lead material have a mean free path on the order of centimetres (to which the blanket is at least 1 order of magnitude thicker), which explains the shrinking of the peak observed at 14.1MeV, and the overall shift to lower energies considering the scales on the x-axis.

A tritium breeding ratio (or TBR- tritons bred per D-T fusion reaction in equation 1) of more than 1 is required for fuel self-sufficiency. With that in mind, the need for Li-6 enrichment becomes clear when figure 1.1.3 is compared with the neutron spectra in the previous two figures.

Li-7 interactions (equation 3) are endothermic and have a threshold energy of around 2.8MeV- higher than the majority of neutron energies after scattering. Li-6's natural abundance is only 7.4% (the rest Li-7), however a typical enrichment for Li-6 in tritium breeding applications such as these is around 60% in order to utilise the large cross section observed for low-energy neutrons, which access tritium breeding interactions via equation 2 with Li-6.

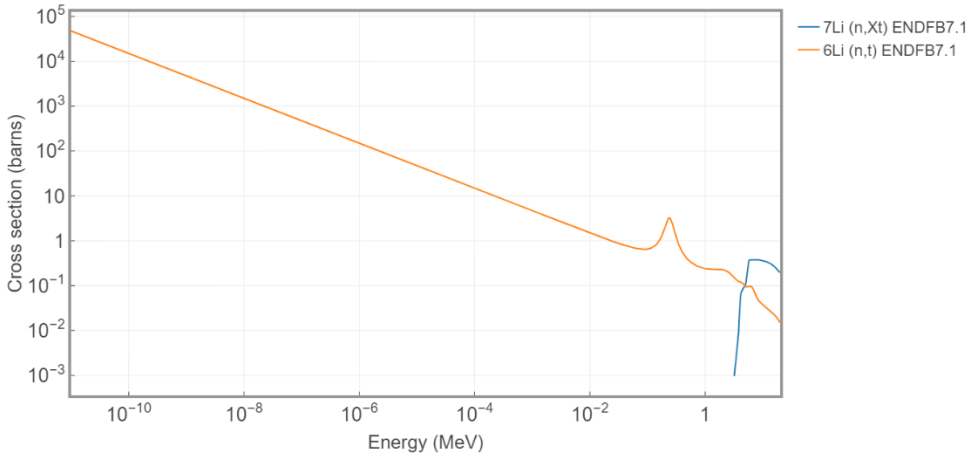

Fig 1.1.3: A plot of the cross section (recorded by ENDFB7.1 Nuclear Data library) for each main tritium-breeding reaction (orange: equation 2, blue: equation 3) on neutron energies.

The cross-section (plotted in figure 1.1.3) is defined as the area transverse to the neutron's relative motion within which it must meet an atom of lithium in order to interact. As each of the nuclei's

radii are on the order of magnitude of 10^{-14}m, the cross section would be expected to be ~10^{-28}m^2, or ~1 barn, if collision simply lead to interaction. The cross-section, as defined here, can act as an expression for the likelihood of interaction from this point onwards.

However, purely accessing tritium breeding via equations 2 and 3 is insufficient to ensure a TBR greater than 1. This is due to a number of factors, such as absorption of expelled neutrons in structural materials, passing through without interaction, or gaps in the blanket structure due to access ports, etc.

Neutron multiplication is therefore required to replenish neutrons that do not interact with the blanket. The following endothermic reaction captures and multiplies some of the fast neutrons (with a threshold of about 7.5MeV). Many compounds are considered for the task, each with different energy multiplication implications in the blanket when considering equation 2 alongside it. In the lithium-lead example given previously the following reaction provides neutron multiplication:

$$ {}^{1}_{0}n_{(fast)} + Pb \rightarrow 2\,{}^{1}_{0}n_{slow} + Pb - 8MeV \qquad \text{(eq. 4)} $$

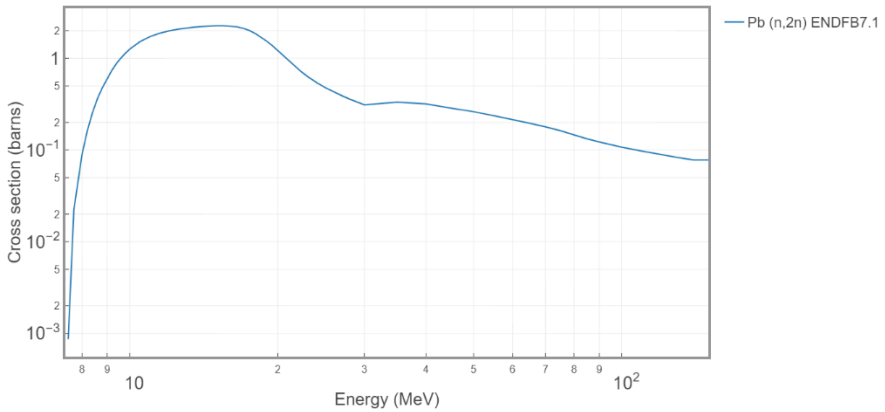

Fig 1.1.4: A plot of the cross section (recorded by ENDFB7.1 Nuclear Data library) for the neutron multiplication reaction in equation 4 on neutron energy.

The two output, slower neutrons are most likely to interact with Li-6 through equation 3. On the whole, about 90% of all tritium bred is due to interactions with Li-6, as reported by Serpent 2 output files (see section 2.1) and in experiment.

The consistent goal for fuel self-sufficiency in the design of DEMO is to keep the 'tritium breeding ratio' (TBR- Tritons bred per D-T fusion reaction, hence tritium fuel used) greater than 1.1- which includes a margin to account for various errors[1]. Tritium storage issues do also impose that the value should not be too far in excess of 1.1, but this is not usually the limiting factor for these studies, and would be simply overcome by removing blanket modules.

1.2 Aims of Study

One factor that has the potential to reduce the TBR value beyond a tangible value is the placement of access ports, which are essentially gaps in the tritium-breeding blanket materials (see section 1.1). Access ports are necessary for run-time diagnostics and other areas, if they are pursued, such as neutral beam heating; a good understanding of their impact on tritium breeding is essential in the design of DEMO to achieve a TBR value greater than 1.1.

This study acknowledged work done by Jenkins, Surrey and Zheng on the impact of Neutral Beam Port location on the TBR[2], but focuses on developing an alternative method of modelling the

scenario to capture and study the entire geometry, and therefore any interactions between multiple ports. The study will aim to compare the TBR values for many different tokamak designs quickly and cheaply, ultimately to assess whether ports interact with one another depending on their geometries to affect the TBR, or how far it is the surface area removed by different port placements that dictates the drop in TBR.

A secondary goal that follows for this study is to demonstrate the power of automated 3D Computer Aided Design (CAD) model generation for the testing of some of DEMO's design points. This can firstly cheaply provide useful pointers for the direction of future, more time-consuming studies. Alternatively, there are some efforts to produce even more sophisticated designs with parameterised, automated 3D CAD scripts, which could begin to replace the current method of manual model construction in 3D CAD software all together in the future. If that direction is pursued in the field, studies such as this will be increasingly useful and be able to produce increasingly directly-informative results.

In the following section, the method pursued for studying the effect of port placement on TBR will be outlined, before presentation of the results and a discussion is conducted around these.

2 - Method

The aim of this study was to gather results about the entire reactor system's geometry, and capture information about neutronics interactions that could not be easily studied analytically. A full scheme of work including computer programs used is available in appendix 3, however this section will outline the scientific method pursued to achieve the aim.

2.1 Computer Aided Design of Models

2.1.1 The NOVA-II Tokamak Model

With new developments in methods of generating cheap 3D CAD models of DEMO comes the opportunity to produce designs with finer differences than have been examined previously in the same time-frame.

For this study, a 3D CAD model of DEMO was produced by a code called NOVA-II [see acknowledgements section]. As presented in figure 2.1.1, NOVA-II produces individual Stereolithography (STL) geometry files for all the essential components of the DEMO reactor, parameterised by user-input values for the tokamak and plasma. This process is cheap enough to be carried out on a personal computer in a matter of minutes. This is far faster than it could take for manual design of a more detailed 3D CAD model, or for the conversion of CAD to more detailed CSG models which are typically used in neutronics studies.

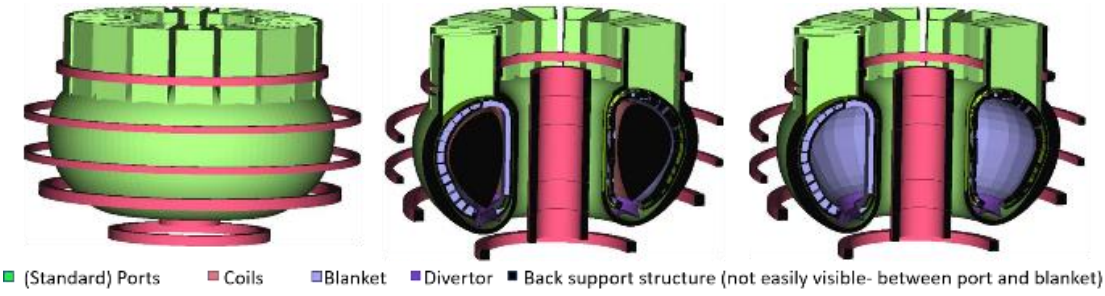

Fig 2.1.1: The output of NOVA-II visualized, from left to right: wholly, cut at y=0, and cut at y=0 with the plasma source removed for visibility.

This study did not use NOVA-II to produce multiple parameterised designs of the tokamak, rather, it should demonstrate the potential of studies that may do so. For this study, a single model of the tokamak was produced with parameters detailed in appendix 1, and this was used in the following processes.

2.1.2 Port Design

In keeping with the study's goal of demonstrating the power of performing cheap tests on automated CAD models, a script was written to produce and manipulate the placement of basic access ports using the 'FreeCAD' libraries within the programming language 'Python'. Figure 2.1.2 shows the port design used in this study.

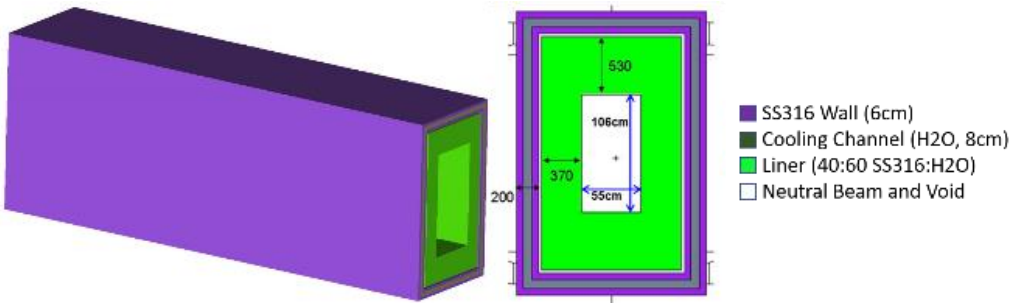

Fig. 2.1.2: 3D CAD representation of the ports, with its dimensions. Ports were 5m long before cutting into the tokamak (see final paragraph in this section). Material cards are detailed fully, by element, in appendix 2.

The ports produced could be positioned at any chosen radial position around the torus and at any lateral position around the outer part of the 'D' cross-section at that radial position (see figure 2.1.3 for a visualisation). Ease of model production in this manner allows for a large quantity of desired designs to be studied quickly and cheaply.

68 port models were successfully produced by this method. These comprised of 2 groups of 3 'base-cases', the first 3 of which had 4 ports. Once some initial tests had been run and it was clear that differences in TBR values between models were marginal (see beginning of results section), another 3 base-cases were produced with 16 ports each, with an aim to enunciate any effects on the TBR value between designs.

The first base-case ('NumberOfPorts.1.' extension) for each group was a radially uniform spread of the ports around the tokamak; the second ('NoP.2') uniformly bunched ports around the quarter-circle points (ie leaving 4 large portions of the blanket uninterrupted between 4 'bunches'); the final base case ('NoP.3') was non-uniform, in that 3 (or 1) ports were placed on one side in the 16 (or 4) port model, with the rest placed on the opposite side. This left 2 large uninterrupted blanket sections around the tokamak.

These base-cases then had their ports' lateral positions adjusted: first uniformly shifted from [-1.0^c, 1.0^c] in intervals of $\frac{2c}{3}$ ('NoP.BaseCase.x' extension, x increases from 1 to 4, with equal intervals from [-1.0^c, 1.0^c]); secondly revisiting each of these angles and negating every other lateral angle ('NoP.BC.x.a' - i.e. so that subsequent ports alternate about the equator), and also producing two (largely inconsequential) randomised models for each base case ('NoP.BC.r1/2' extensions). The final adjustment made was to produce some forms of the radially non-uniform models in which ports on opposite sides of the tokamak had oppositely-signed angles ('NoP.3.oy' extension, with y=[1,5] increasing with equal intervals from [-1.0^c, 1.0^c]). Figure 2.1.3 gives a visual representation of each of these cases.

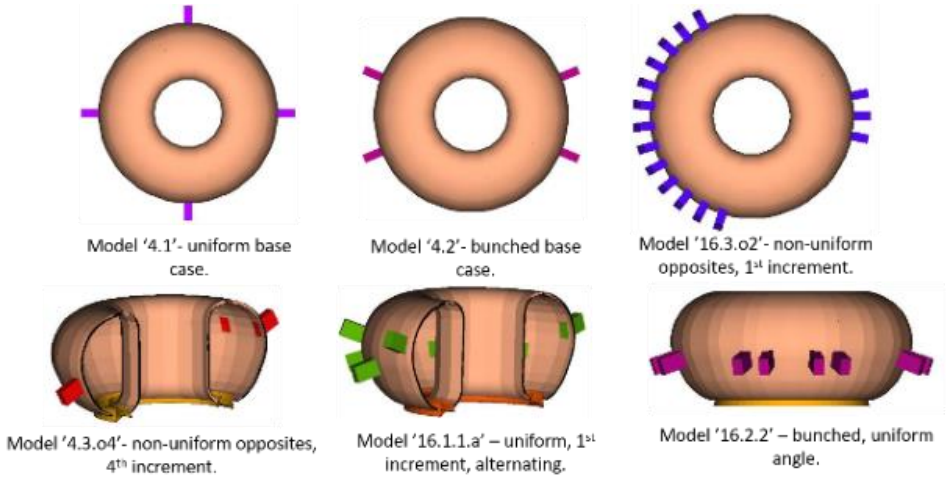

Fig 2.1.3: A representation of a selection of cases studied, only showing the back support structure, divertor, and access ports for ease of viewing.

As visualised in figure 2.1.3, once a port model was obtained, Boolean Operations were performed on the tokamak geometry generated in section 2.1.1 to 'cut holes' in the original model around the outline of the now-placed ports, and the ports were inserted into that model. This was all performed by scripts run on a personal computer and was the full process for producing a model to be studied.

2.2 Simulation

Once a model was obtained through automated CAD scripts as detailed in section 2.1, it was ready to undergo the neutronics simulation described in this section.

2.2.1 'Serpent' Code

This study made use of a Monte Carlo neutronics code called 'Serpent 2'[3], which makes use of nuclear data libraries for the materials specified in its input file and tracks the motions of a specified number of neutrons from a specified source (the plasma, in this case) before feeding back data about various interactions of neutrons, photons, etc, as it is requested. Serpent features the ability to read in user-provided STL geometry files (as used for model representation in this study).

In this study we are most interested in tracking those neutrons that result in the breeding of a Triton. This can be achieved by specifying 'macroscopic detectors' of all cases of tritium breeding in the geometry (hence 'macro'). 'Microscopic detectors' correspond to the user specifying the materials to monitor for the event of the specified interaction in those materials only. Although measured, this will not be presented in this paper, as the relative statistical error returned was larger for these data and, furthermore, similar trends were mirrored in each output dataset. Overall, there was no use for this microscopic detection.

Again, an automatic script was produced that read in all the STL files in a model directory and associated materials with components identified by filename-prefixes, allocated as shown in figure 2.2.1. The nuclear data library 'FENDL3.1b'[4] was used (as well as 'JEFF'[5], for isotopes of Sulphur).

Component	Material Used
Plasma	Plasma
(Standard) Ports	'Eurofer'
Back support structure	'Eurofer'
Divertor	Homogenised Divertor Material
Coils	Homogenised Magnet Material
Blanket	$Pb_{84.2}Li_{15.8}$

Fig 2.2.1: The materials associated with each component generated by NOVA-II (see figure 2.1.1). For a full break-down of each material used, by element, see appendix 2.

Once the input file was created, this was submitted to a computer cluster to simulate the number of neutrons required to keep statistical error low while keeping to a feasible amount of time (see section 2.2.2). Serpent ran the simulation and produced a detector output file holding information about the ratio of neutrons that reacted to result in the breeding of a triton to those released by the source- in other words the TBR value. The results collected from these files are presented in section 3.

2.2.2 Error Considerations in Simulation

The first consideration to make is over the validity of the Serpent code output. The output received in this case was a ratio of neutrons that were involved in an n + x -> T + y reaction in the system to the number output by the plasma source. This study relies on a number of thorough benchmark studies[6] performed by writers of the Serpent code and others, for these means.

One source of error that one does have an element of control over is statistical error. Total Monte Carlo simulations' precision increases roughly with $1/\sqrt{N}$, where N is the number of neutrons simulated. N was to be decided by a compromise between the time taken to run each simulation (in order to satisfy the study's goals) and the relative error returned. Test runs were performed to prove this relationship and gather information on the statistical error returned, as seen in figure 2.2.2.

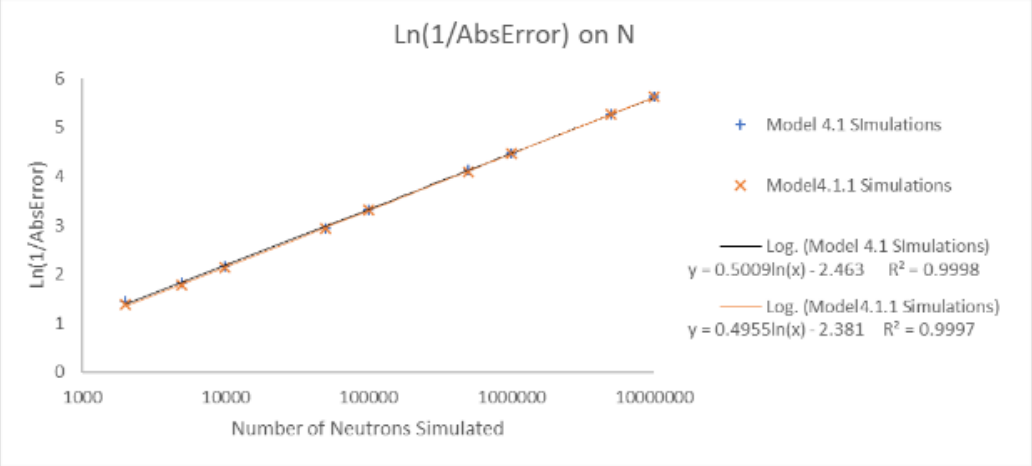

Fig 2.2.2: A log-graph tracking the absolute error on a simulated TBR value with the number of neutrons selected for simulation. The gradient of ~0.5 confirms the predicted $1/\sqrt{N}$ relationship.

A change in TBR of 0.01 is thought to be significant, and it was found that 5 million neutrons gave a relative error in the TBR value of < 0.005. Although doubling the number of neutrons did improve relative error, it was decided that 10 million neutrons would likely be excessive, in terms of other errors overshadowing statistical error (see section 4.2), as well as increase the resources required.

All generated models (section 2.1.2) were subjected to the neutronics simulations, and in the following section the results of these simulations are presented.

2.3 Surface Area Retrieval

Using the 'FreeCad' libraries, a script was produced that would identify blanket modules and deduce which of their (up to 100s of) faces were plasma-facing. This was achieved by examining dot-products between the unit normal to the face and the unit vector between the plasma-centre and the face's centre of mass, taking only those dot products within 15% of the max dot-product for that module.

Correct face identification was verified by checking against 'standard' modules in various positions which had a certain total number of faces (12), of which there were always another number (2) of front faces to check the script had identified exactly.

3 - Results

After simulation described in section 2.2, the macroscopic tritium breeding detector data is collected to obtain the number of Tritons bred per simulated neutron to obtain a result for the TBR directly. A representation of all results is given in figures 3.0.1 and 3.0.2.

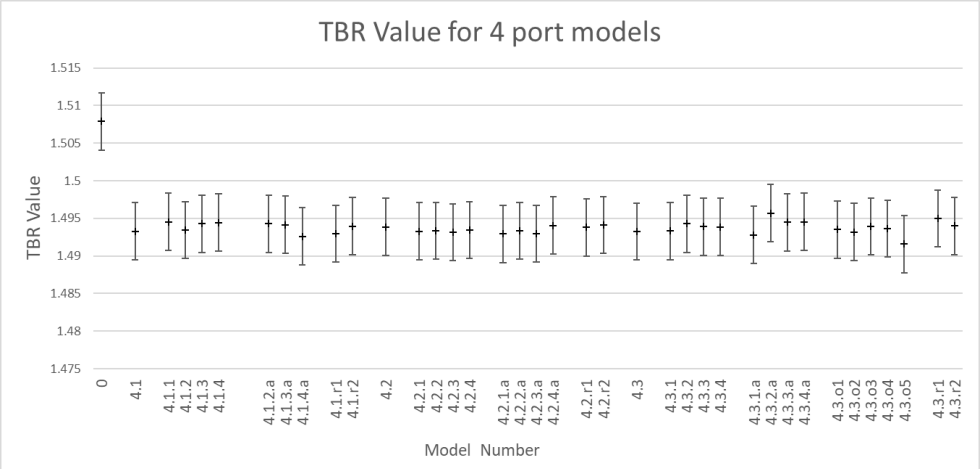

Fig 3.0.1: The results for 4-port models (and the 0-port base case, taken as a NOVA-II reference). Models of the same type are collected into bunches. See section 2.1.2 for an explanation of model types and nomenclature.

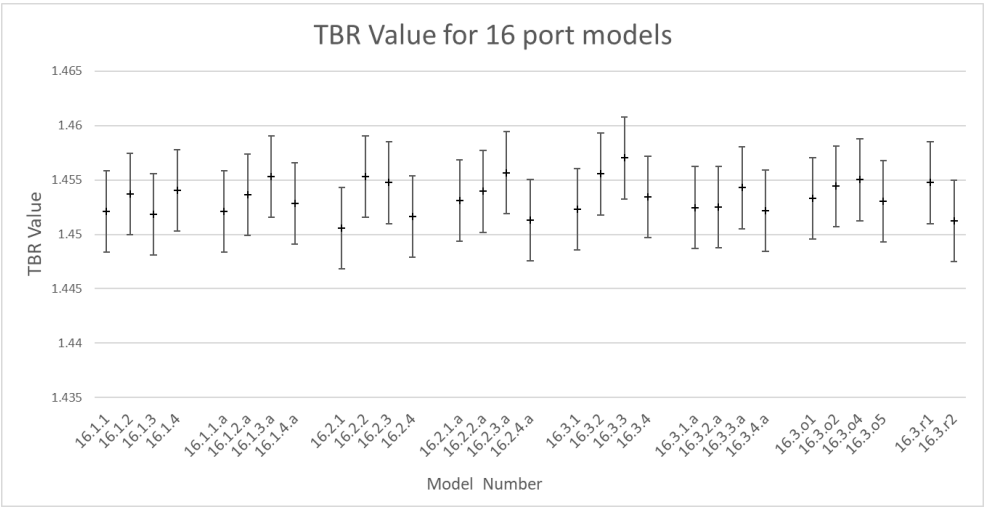

Fig 3.0.2: The results for 16-port models. Models of the same type are collected into bunches. See section 2.1.2 for an explanation of model types and nomenclature.

The first observation in these results is the low spread. The largest differences in TBR (between models with the same number of ports) can be observed in the 16-port models, where at times models' TBRs nominally vary by 0.01. As predicted, differences in comparative 16-port models are more enunciated than their 4-port counterparts, but even so the error bars clearly dominate the rather small differences. Intuitively, more holes in the blanket structure (i.e. 16 ports opposed to 4) resulted in a lower TBR value.

The results will now be presented in different groupings in order to examine the data for any patterns that may be present.

3.1 Radially Uniform Models (NoP.1)

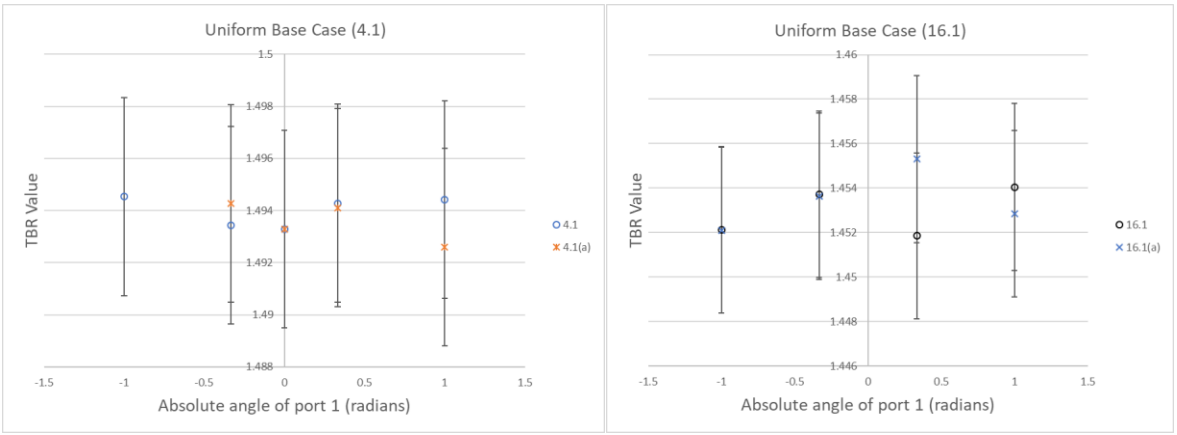

Fig 3.1.1, 3.1.2 (left, right): A graph of the TBR values on lateral port angle for the model with 4, 16 uniformly-spaced ports (see fig 2.1.3 for visualisation). x.1 denotes uniform lateral angle, x.1(a) denotes successive ports' angles alternate in sign (about the equator).

It is difficult to draw conclusions from these results alone, given the size of the error bars; the error on each measurement spans most of the range of every other measurement made for the model. The main observation is that the data points for both the 4-port and 16-port models are (separately) within about 0.01 of each other in TBR, which is less than the amount deemed to be significant.

3.2 Radially Bunched Models (NoP.2)

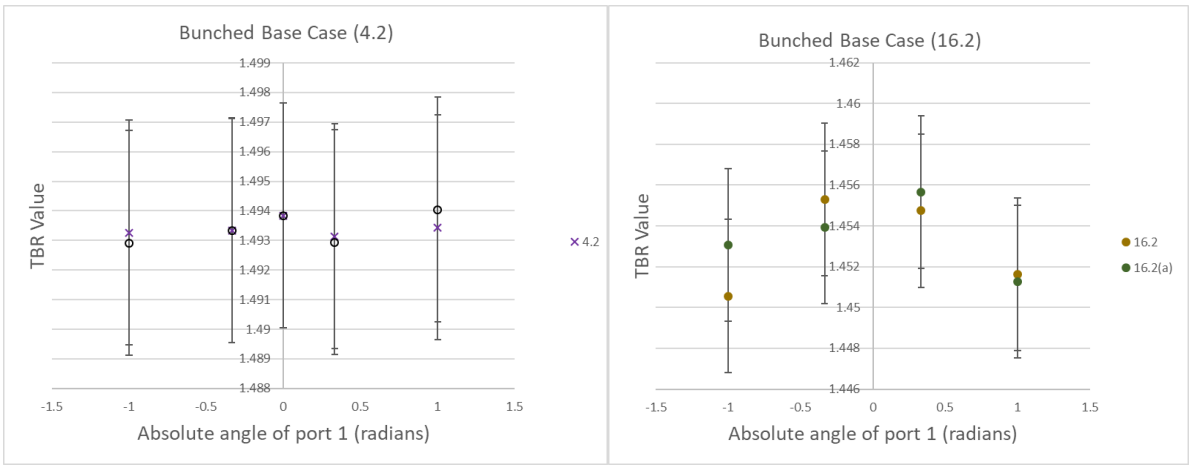

Fig 3.2.1, 3.2.2 (left, right): A graph of the TBR on lateral port angle for the bunched cases (x.2 – see fig 2.1.3). The (a) denotes successive ports alternating in sign about the equator.

Once again, all TBR values conform to within 0.01, however we are now potentially seeing the emergence of a pattern with smaller lateral angles being preferred to larger ones; although of course the error still makes it impossible to draw sound conclusions. More test cases are required.

3.3 Radially Non-Uniform Models (NoP.3)

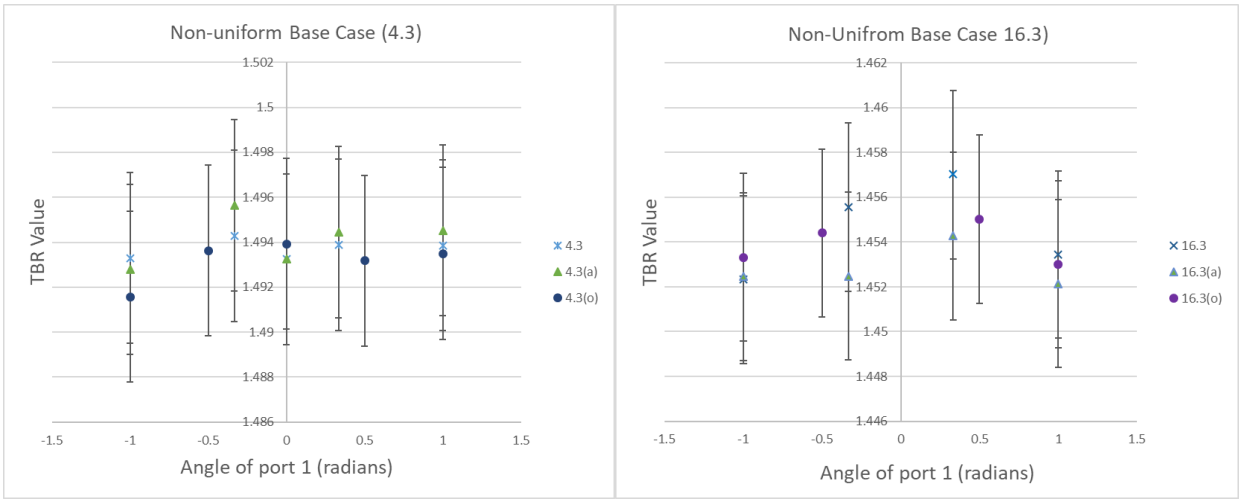

Fig 3.3.1, 3.3.2 (left, right): A graph of TBR values on lateral angle of the smaller group of ports (1, 3), eg in x.3 models (see fig 2.1.3). The larger bunch of ports have the negative of these angles in the (o) models, else angles are alternating (a) or uniform (no extension to key).

Despite the size of the error bars, these data again suggest that smaller lateral angles could give rise to a higher TBR value than large lateral angles, and, perhaps less firmly, equatorial port placement. Coupled with the results in section 3.2, a pattern of the preference of small lateral angles is potentially emerging, even through the large error bars.

Also in this case we potentially see the 16-port model enunciating the effect observed in the 4-port model, as predicted, which is encouraging when considering the (repeated) patterns seen only in nominal values.

The same results are now presented in different groupings to attempt to observe further patterns.

3.4 Laterally Uniform Models (NoP.BC.y)

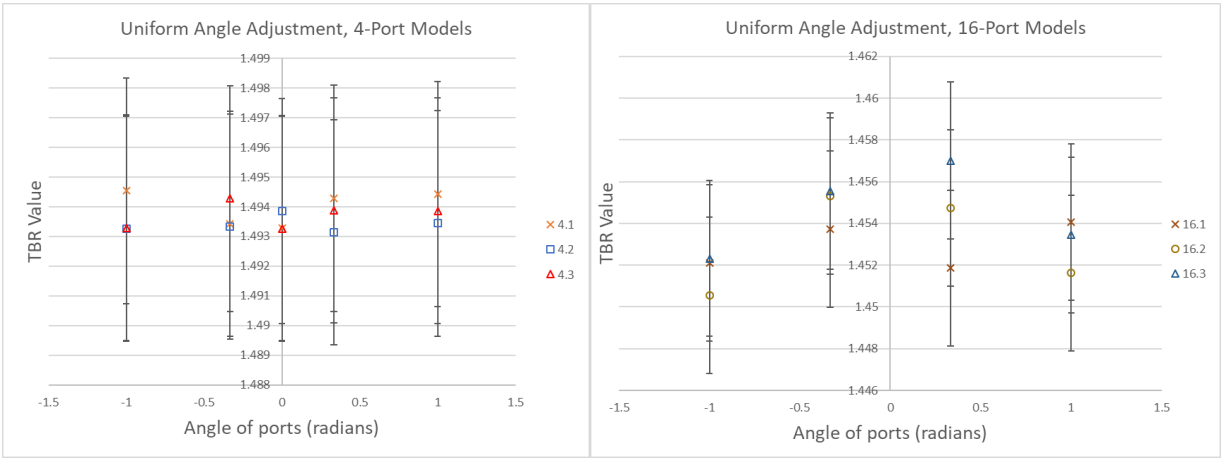

Fig 3.4.1, 3.4.2 (left, right): A graph of TBR on lateral port positioning for all 4, 16 port laterally uniform models. All ports have the same lateral angle in these cases (see fig 2.1.3).

When all uniform models are placed together, the suggestion of a pattern of small lateral angles being more favourable than large positive angles (and possibly equatorial ports) is viewed more readily. Of course, not all data agree with this observation, and the error bars are large enough to make it impossible to draw this as a conclusion, however it is a repeated result.

Also from this graph we may see some favour towards the radially non-uniform model (NoP.3 models), but again further testing would be required to confirm this.

3.5 Alternating Models (NoP.BC.y.a)

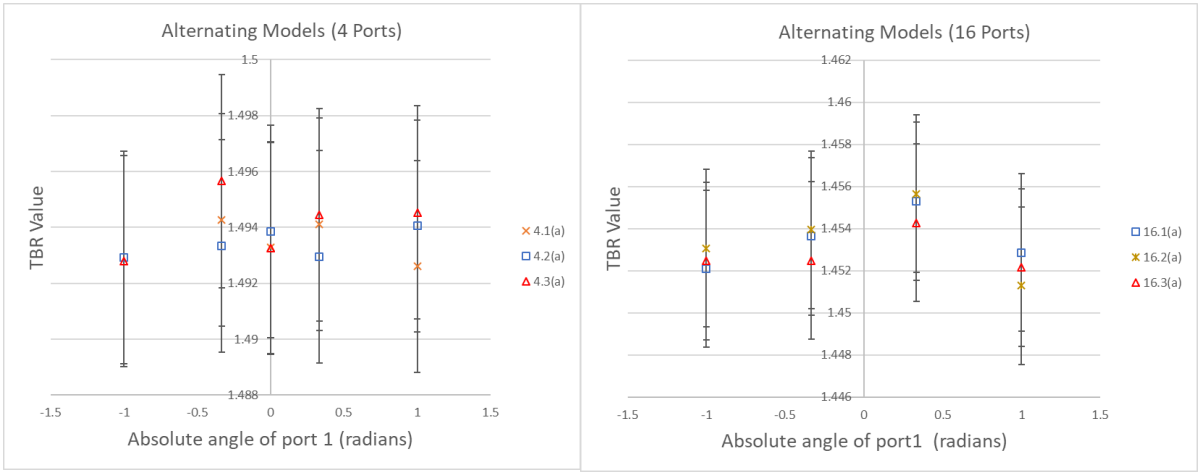

Fig 3.5.1, 3.5.2 (left, right): A graph of TBR on lateral port positioning for all 4, 16 port laterally alternating models. Successive ports have the same magnitude of lateral angle but opposite sign in this case (see fig 2.1.3).

Once again in this representation there is slight suggestion that a small radial angle is preferred over larger angles or equatorial positioning; more testing should be done in this area.

In this case, the alternating 16.3 appears least favourable of the three, however is potentially the most favourable amongst the 4-port models. Few conclusions can be drawn here, if any, with regards to that discussed at the end of section 3.4. A discussion on the effect of port geometries and their interactions takes place in section 4.1.

4 - Discussion

4.1 Interpretation of Results

4.1.1 Interpreting Geometries

The primary observation from this study was that the actual location of the access ports was relatively insignificant, compared with number of access ports. Figure 4.1.1 begins to suggest a reason for such small variations in the TBR.

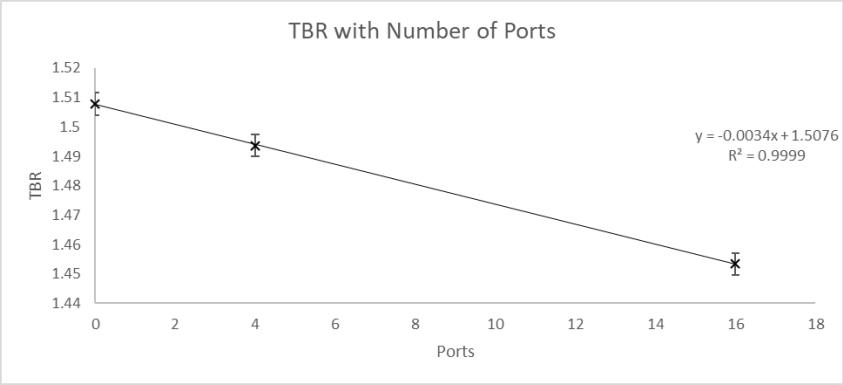

Fig 4.1.1: A plot of TBR value on number of ports. The average TBRs of all models with that number of ports was taken and the standard deviation found for that dataset, then plotted above.

The averaging of every port model should nullify the effect of each port model having their ports in different positions (and similar patterns were observed when taking single models of the same base-case). The lack of skew in figure 4.1.1 suggests that additional ports do not interact with other ports within an 'average' model; or, to reiterate, there may be no additional gain or drop in TBR due to interactions between ports, only a set change in TBR due to a change in blanket area exposed.

If that result is extrapolated to consider what happens between ports in a single model, it is imaginable that the position of one port has little impact on the TBR loss induced by another port, hence there is little difference between most models in which the ports are in a similar position, and inter-port interactions are not readily observed. There is a discussion following on from this argument in section 4.1.2.

The pattern emerging from the results (specifically sections 3.3 onwards) did appear to show a preference towards small lateral angles over larger ones, and then (to a lesser degree) the preference of a small lateral angle over an equatorial port, also.

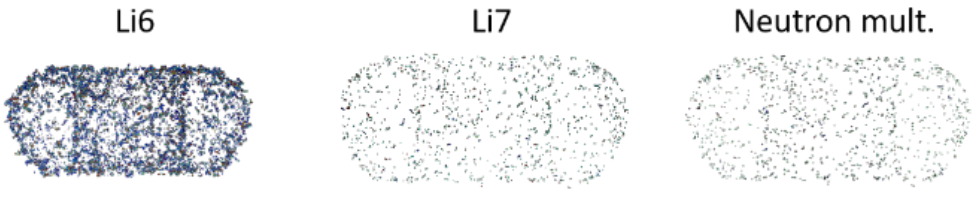

Fig 4.1.2: A map of all neutron collisions undergoing specified interactions (labelled). These figures are output during the simulation by Serpent 2.

One hypothesis for preference of small lateral angles (if this is indeed the case) can be deduced from figure 4.1.2; if more neutron collisions take place in the region around the equator and at about 1 radian from the equator, and fewer take place between these regions, then the region in between is the preferential region in which to place an access port. This could be backed-up by an argument around the surface area available for interactions in these areas, as will be discussed in the following sub-section (4.1.2).

More testing would required to confirm these arguments, of course, as all patterns 'observed' in this study are over-shadowed by the error bars (or perhaps more accurately, are difficult to observe due to small differences in the TBRs). Other errors in this study will be discussed in the following section (4.2).

Despite the difficulties with small variations in TBR values, these results were in line with study's aims; the beginnings of a pattern has emerged at a low cost. With more resources and time, this pattern could be probed more closely, and this study could serve as a useful starting point.

4.1.2 Investigating Surface Area and TBR

After simulation, the surface area of all front-facing blanket module faces was retrieved from the model's file directory (see section 2.3) and plotted with the TBR for that model.

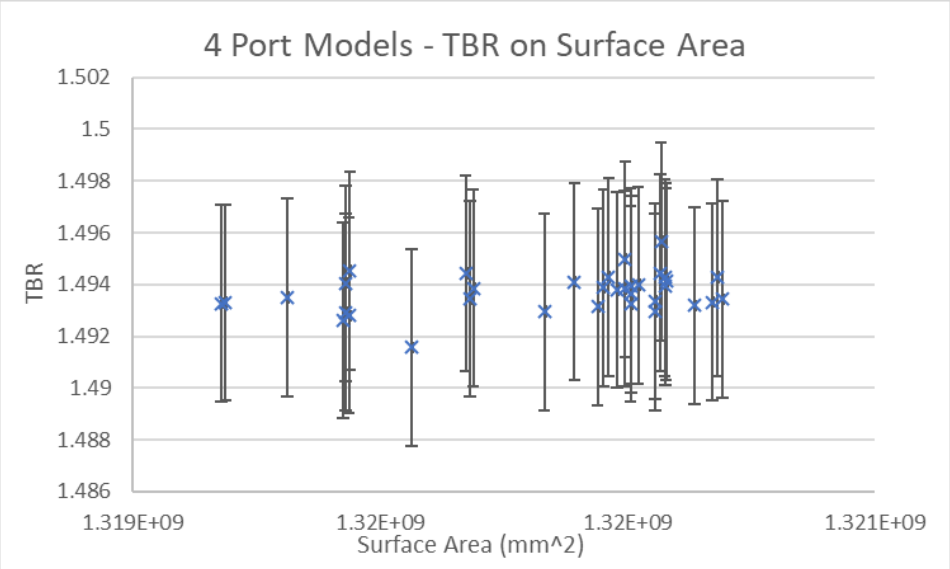

Fig 4.1.3: A graph of the TBR values simulated on the retrieved surface areas of all front-faces belonging to blanket modules in 4-port models.

As it is clear from figure 4.1.3, the 4-port models did not show much meaningful correlation between the total blanket front-face surface area and the TBR result. Again, the 16-port models appear to enunciate effects on the TBR, so the following figure will be the focus of this sub-section's discussion.

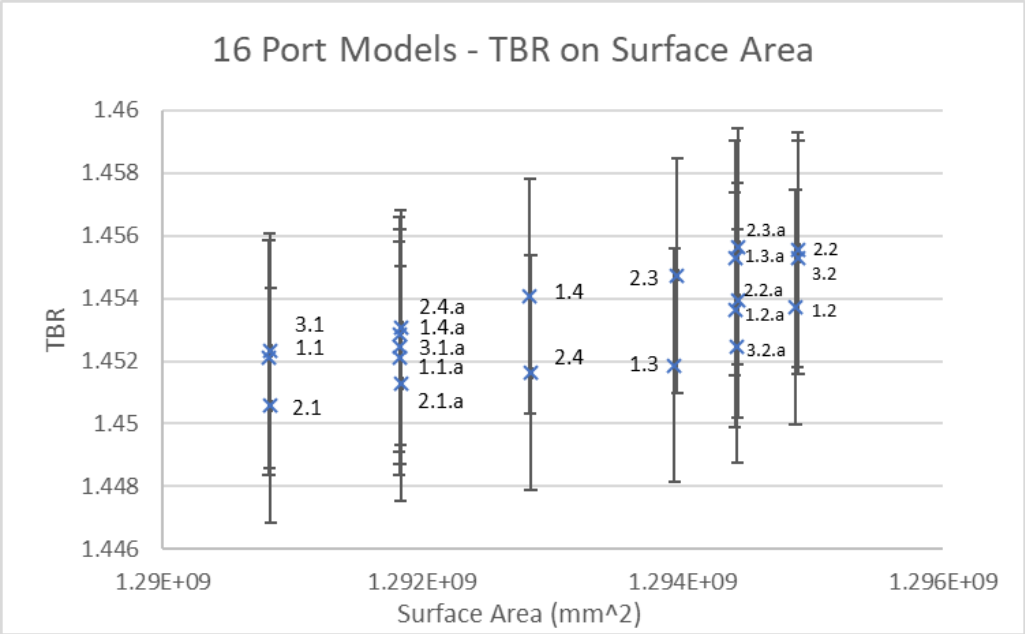

Fig 4.1.4: A graph of the TBR values simulated on the retrieved surface areas of all front-faces belonging to blanket modules in 16-port models. See section 2.1.2 for naming conventions- each label assumes the 16-prefix implicitly (e.g. 3.1 -> 16.3.1).

Once again, when examining the 16-port models (figure 4.1.4), a pattern begins to emerge. As one may have predicted, a general upwards-trend is revealed between TBR and surface area exposed to the plasma.

It is however difficult to conclude whether surface area is the sole driving force behind differences in TBR, once again due to the size of the statistical error in the Monte Carlo simulations, or whether the port geometries interact to lower the TBR in certain cases where the surface area has increased (for example between the '2.4' and '2.4.a' data-points, which are within statistical error of showing an increase in TBR, but nominally show a decrease).

It should also be noted that the grouping of the 3 largest surface areas in figure 4.1.4 correspond to the models with a small lateral angle, and the grouping of the 3 smaller surface areas correspond to a large lateral angle. This could provide an explanation for the observation discussed in section 4.1.1- that a small lateral angle is favoured over a large one. There are, unfortunately, no TBR data for equatorial 16-port models to deduce if more surface area is use by equatorial ports than small lateral angled ports (hence suggesting a preference for the small lateral angle).

Overall, though, this discussion is focusing on very small (less than 0.005) changes in the TBR for relatively large geometric changes in the models (eg adjustment of port angle, radial position etc). Although the data cannot be conclusive in the extent to which ports interact within a model, the surface area effect is noticeably present over blanket coverage area changes of $5 \times 10^{6} mm^{2}$ (or $5 m^{2}$), as spanned in figure 4.1.4.

If it is concluded that the differences in TBR observed are due to model differences (i.e. not statistical error, else the data is very weakly correlated), these data suggest that the drop in TBR per m^{2} of blanket coverage removed is $7 \times 10^{-4} m^{-2}$ on average within the 16-port model range, which could be significant when considering future DEMO design.

4.2 Non-Statistical Errors

4.2.1 Data Errors

The largest source of error in this study arises from the fact that the only quantifiable errors involved were those introduced statistically by the Total Monte Carlo simulation. Errors in the nuclear data are not readily accessible, therefore these were treated as nominal values throughout.

This could a major shortfall for any study involving nuclear data libraries, however the study may still stand as a useful comparison study; the data have at least been referenced to rule-out major calculation error in line with the *"Guidelines for Nuclear Data Verification and Validation"* [7].

Secondly, particular to this study, an homogenised blanket material was used (see appendix 2), hence any imbalance in neutron multiplication and Tritium breeding reaction probabilities would be the same for all models used, and this error would be relatively insensitive to the particular geometry of each model due to this homogeneity; the interaction locations do not depend on the geometry of the model any more than where the material is missing due to a port being located there, as far as the code is concerned.

4.2.2 Geometric errors

As well as a strength in terms of ability to perform cheap tests, loss of sophistication is a draw back of quick, automated CAD design. Models still currently lack some details, which restricts this study to be comparative between models rather than give an idea on how DEMO will actually operate.

A second draw back, specific to this study, is the method used required a structure with no gaps in the STL geometry in order to cut off the port and prevent over-hang into the plasma. The inner-most structure in the NOVA-II model with this property was the back support structure, which led to problems as seen in figure 4.2.1.

Some comparisons can still be made as, firstly, a minimal number of neutrons will hit the unprotected inner-blanket region, and secondly all models were exposed to the same issue.

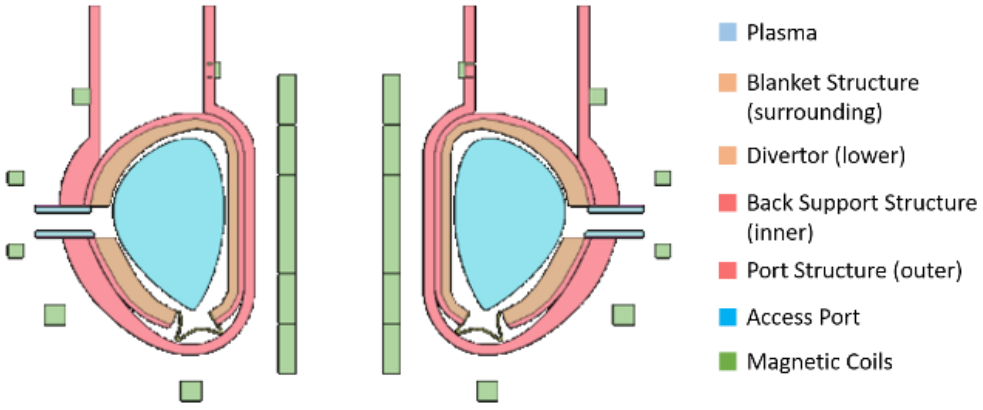

Fig 4.2.1: An output file from the Serpent 2 simulation. See the added ports on the left and right do not extend through the blanket structure, and had to be cut at the back support structure.

4.3 Future Improvements

4.3.1 Statistical Error

A natural improvement to the study would be to increase the number of neutrons to decrease statistical error (which goes with $1/\sqrt{N}$).

This study reduced the absolute error in TBR to half the value of significance (deemed to be ~0.01), but to form firmer conclusions on the patterns discussed in section 4.1, smaller error bars would be useful. However, at that point, uncertainty in the nuclear data would be the study's main restriction (if it is not already, depending on the size of these unknown uncertainties).

4.3.2 Nuclear Data Errors

There is certainly scope to add uncertainties to nuclear data used in studies such as these to the errors in these results, however this is not a simple procedure and work is currently being done in this area[8, 9]. To do so would greatly increase the expense of studies such as these, but would be ultimately necessary when designing DEMO.

4.3.3 Geometric Impovements

Finally, geometric improvements could be made on the problems outlined in the previous section, but this study's aim was to perform a cheap test; spending further time on these issues would have been beyond the aims of this cheap comparison study.

5 - Conclusions and Future Study

Ultimately, this study will be limited by the lack of errors on the nuclear data used. As it stands, the study serves as a cheap test to begin to probe some patterns in favourable port positioning around the EU DEMO tokamak, and draw some conclusions over inter-port interactions.

Although all simulations produced comparative TBR values within the significant limit of around 0.01 of each other, the study points towards the optimal lateral access port positioning to be off the equator, with a small lateral angle. This was backed up in the surface area data, where these models were shown to have a smaller reduction in surface area than those with a large lateral angle.

More time should be spent in reducing statistical errors in this study, or producing more models in the range of lateral angles examined, to test that hypothesis more thoroughly. If the hypothesis were proven this could have important implications for future EU DEMO designs to maximise the TBR obtained.

The results were inconclusive over which of the three radial models examined was optimal. They were also inconclusive over whether the ports within a model's geometry interact meaningfully at all, but there is a suggestion that surface area is the overriding factor in TBR losses with the conclusion that this dictates the preference for a small lateral angle.

More time could be spent in simulation to reduce statistical errors in the results and probe any patterns that may have emerged in the radial models, or more time could be spent producing models to cover a larger range of surface areas (such as by varying port dimensions) to specifically make stronger conclusions on the effect of surface area losses. A combination of the two may be preferable.

Ultimately, however, the reason the statistical error was too large to make conclusions from these data is because the differences in TBR for a given number of ports used in this study in any geometry used was small, to the point of insignificance (less than 0.01 in all cases). This is, of course, an important conclusion in itself for practical means of design.

If the study were to be refined further in order to probe finer differences, it may finally be interesting to study whether a positive or negative lateral port angle was preferred. Some preference would be expected- the non-uniform curve of the tokamak 'D' shape suggests more or fewer neutron interactions would take place (or m^2 of surface area would be available) on each side of the equator- this was not observed consistently in this study, however.

Acknowledgements

I would finally like to acknowledge each of those that made this research project possible.

First I give my thanks to Dr. Jonathan Shimwell for his diligent supervision and generous giving of his time for the duration of the project, without which I could not have surmounted the learning-curve and completed such a study in the time available to me.

Secondly I'd like to recognise Simon McIntosh for his writing of the NOVA-II code, and Samuel Ha and Samuel Merriman for their efforts and subsequent help in improving and making available the NOVA-II code, particularly for this study.

I am also grateful for the free availability and support offered with Serpent 2, written by J. Leppänen et al.

Finally, I would like to thank my college, St John's College, Cambridge, for their financial support with my accommodation costs for the summer.

References

[1] **Laila A. El-Guebaly, Seigfried Malang (2009)** *"Toward the ultimate goal of tritium self-sufficiency: Technical issues and requirements imposed on ARIES advanced power plants"* Fusion Engineering and Design, Volume 84, Issue 12, p2072-2083

[2] **I Jenkins, E Surrey, S. Zheng (2014)** *"The Impact on Tritium Breeding Ratio of Neutral Beam Port Location in DEMO"* FIP/P7-5

[3] **Leppänen, J., et al. (2015)** *"The Serpent Monte Carlo code: Status, development and applications in 2013."* Ann. Nucl. Energy, 82 (2015) 142-150.

[4] **D. W. Muir, S. Ganesan, A. B. Pashchenko (1991)** *"FENDL: A Reference Nuclear Data Library for Fusion Applications"* Nuclear Data for Science and Technology pp 933-935

[5] **K. Shibata, O. Iwamoto, T. Nakagawa, N. Iwamoto, A. Ichihara, S. Kunieda, S. Chiba, K. Furutaka, N. Otuka, T. Ohsawa, T. Murata, H. Matsunobu, A. Zukeran, S. Kamada and J. Katakura (2011) "***JENDL-4.0: A New Library for Nuclear Science and Engineering",* J. Nucl. Sci. Technol. 48(1), 1-30

[6] **Leppänen, J., Aufiero, M., Fridman, E., Rachamin, R., and van der Marck, S. (2014)** *"Calculation of effective point kinetics parameters in the Serpent 2 Monte Carlo code."* Ann. Nucl. Energy, 65 272-279

[7] **A. Trkov (2005)** *"Guidelines for Nuclear Data Verification and Validation"* INDC(SEC)-0107

[8] **D. Rochman, ∗ A. J. Koning and S. C. van der Marck (2011)** *"Exact Nuclear Data Uncertainty Propagation for Fusion Design"* Journal of the Korean Physical Society, Vol. 59, No. 2, pp. 1386~1389

[9] **F. Thomas, M. Fleming (2017)** *"Quantifying TBR uncertainty due to lead nuclear data in HCLL blanket modelling by the Total Monte-Carlo method"* Fusion Engineering and Design 0920-3796

Appendices

1 Plasma Parameters Used

T = 15.4K
Major Radius = 8.801733731571085m
Minor Radius = 2.82876968374109m
Elongation = 1.4890553256601347
Triangularity = 0.30525547503188875
Offset from wall = 1.07ψ
Divertor grazing angle = 1.5°

2 Material Cards

All materials are presented in the given format:
(ZZZAAA, mass_fraction)
Ie (00)8016 is Oxygen-16. Preceding '0's are not presented in this format.

Eurofer

Density: 7750kgm^{-3}
(26054, 4.56563E-03), (26056, 6.91110E-02), (26057, 1.56807E-03), (26058, 2.05084E-04), (5010, 9.43123E-07), (5011, 3.45108E-06), (6012, 4.14310E-04), (7014, 1.34911E-04), (7015, 4.65085E-07), (8016, 2.95487E-06), (13027, 7.02121E-06), (14028, 4.05884E-05), (14029, 1.98991E-06), (14030, 1.26804E-06), (15031, 3.05762E-06), (16032, 4.21784E-06), (16033, 3.27443E-08), (16034, 1.79397E-07), (16036, 7.89886E-10), (22046, 8.49986E-08), (22047, 7.50223E-08), (22048, 7.27880E-07), (22049, 5.23259E-08), (22050, 4.90993E-08), (23050, 4.651675e-8), (23051, 0.00001856018), (24050, 3.70662E-04), (24052, 6.87292E-03), (24053, 7.64630E-04), (24054, 1.86808E-04), (25055, 4.73931E-04), (27059, 4.01637E-06), (28058, 5.56272E-06), (28060, 2.07132E-06), (28061, 8.85630E-08), (28062, 2.77823E-07), (28064, 6.85423E-08), (29063, 1.56104E-06), (29065, 6.74368E-07), (41093, 2.54802E-06), (42092, 2.29342E-07), (42094, 1.39911E-07), (42095, 2.38263E-07), (42096, 2.47037E-07), (42097, 1.39981E-07), (42098, 3.50081E-07), (42100, 1.36919E-07), (73181, 3.14209E-05), (74182, 7.59071E-05), (74183, 4.07659E-05), (74184, 8.68119E-05), (74186, 7.96842E-05)

Homogenised Divertor

Atomic Density: 6.61502E-02 barn^{-1}cm^{-1}
(26054, 5.72333E-04), (26056, 8.66354E-03), (26057, 1.96569E-04), (26058, 2.57087E-05), (6012, 6.00566E-05), (25055, 6.55763E-05), (15031, 9.69542E-07), (16032, 8.91624E-07), (16033, 6.92194E-09), (16034, 3.79233E-08), (16036, 1.66977E-10), (14028, 9.90013E-06), (14029, 4.85370E-07), (14030, 3.09294E-07), (28058, 7.05554E-07), (28060, 2.62719E-07), (28061, 1.12330E-08), (28062, 3.52380E-08), (28064, 8.69364E-09), (24050, 4.96251E-05), (24052, 9.20165E-04), (24053, 1.02371E-04), (24054, 2.50103E-05), (42092, 4.84813E-08), (42094, 2.95762E-08), (42095, 5.03672E-08), (42096, 5.22220E-08), (42097, 2.95910E-08), (42098, 7.40047E-08), (42100, 2.89437E-08), (23051, 2.95000E-05), (73181, 4.64952E-06), (74182, 1.05030E-05), (74183, 5.64064E-06), (74184, 1.20119E-05), (74186, 1.10256E-05), (22046, 2.15618E-07), (22047, 1.90311E-07), (22048, 1.84643E-06), (22049, 1.32736E-07), (22050, 1.24551E-07), (29063, 6.59987E-07), (29065, 2.85114E-07), (41093, 3.23181E-07), (13027, 2.22636E-06), (7014, 1.92505E-05), (7015, 6.63632E-08), (5010, 2.39244E-07), (5011, 8.75444E-07), (27059, 1.01884E-06), (50112, 5.20609E-09), (50115, 1.77721E-09), (50116, 7.53468E-08), (50117, 3.94579E-08), (50118, 1.23382E-07), (50119, 4.33915E-08), (50120, 1.63203E-07), (50122, 2.28128E-08), (51121, 2.84214E-07), (51123, 2.09120E-07), (40090, 3.43638E-07), (40091, 7.41156E-08), (40092, 1.12056E-07), (40094, 1.11143E-07), (40096, 1.75326E-08), (8016, 3.74785E-06), (4009, 4.78827E-02), (3006, 7.26769E-04), (3007, 2.49178E-03), (14028, 7.85504E-04), (14029, 3.85106E-05), (14030, 2.45403E-05), (8016, 3.39845E-03)

Homogenised Magnet

Atomic Density: 7.194x10^{-2} barn^{-1}cm^{-1}
(1001, 3.89340E-03), (6012, 3.40560E-03), (7014, 3.70800E-04), (8016, 4.87080E-03), (12024, 1.69197E-04), (12025, 2.14200E-05), (12026, 2.35834E-05), (13027, 7.07400E-04), (14028, 1.32800E-03), (14029, 6.72000E-05), (14030, 4.46000E-03), (16032, 8.71457E-05), (16033, 6.97680E-07), (16034, 3.93822E-06), (16036, 1.83600E-08), (29063, 6.83585E-03), (29065, 3.05684E-03), (41093, 1.18439E-03), (50112, 3.82953E-06), (50114, 2.60566E-06), (50115, 1.34231E-06), (50116, 5.74035E-05), (50117, 3.03204E-05), (50118, 9.56198E-05), (50119, 3.39131E-05), (50120, 1.28625E-04), (50122, 1.82791E-05), (50124, 2.28587E-05), (2004, 3.08888E-03), (5010, 4.06294E-07), (5011, 1.48738E-06), (6012, 1.70203E-04), (7014, 2.77382E-04), (8016, 2.55621E-06), (13027, 2.27302E-04), (14028, 7.27891E-05), (15031, 1.65004E-05), (16032, 8.47338E-07), (16033, 6.78371E-09), (16034, 3.82922E-08), (16036, 1.78519E-10), (19039, 2.43807E-07), (19040, 3.05877E-11), (19041, 1.75950E-08), (22046, 1.40904E-06), (22047, 1.27070E-06), (22048, 1.259086E-05), (22049, 9.23990E-07), (22050, 8.84708E-07), (23050, 4.013075e-9), (23051, 0.00000160121), (24050, 3.03427E-04), (24052, 5.67045E-03), (24053, 6.34294E-04), (24054, 1.55150E-04), (25055, 5.58169E-04), (26054, 1.46579E-03), (26056, 2.21899E-02), (26057, 5.16004E-04), (26058, 7.24415E-05), (27059, 1.73444E-05), (28058, 2.89354E-03), (28060, 1.07976E-03), (28061, 5.07463E-05), (28062, 1.46193E-04), (28064, 4.48851E-05), (29063, 2.24477E-05), (29065, 9.72920E-06), (40090, 2.30510E-07), (40091, 5.02686E-08), (40092, 7.68366E-08), (40094, 7.78671E-08), (40096, 1.25448E-08), (41093, 1.21022E-05), (42092, 6.32488E-05), (42094, 3.94240E-05), (42095, 6.78518E-05), (42096, 7.10910E-05), (42097, 4.24074E-05), (42098, 1.02843E-04), (42100, 4.10435E-05), (50112,

3.34089E-09), (50114, 2.27319E-09), (50115, 1.17103E-09), (50116, 5.00790E-08), (50117, 2.64516E-08), (50118, 8.34190E-08), (50119, 2.95859E-08), (50120, 1.12213E-07), (50122, 1.59467E-08), (50124, 1.99420E-08), (73181, 5.64891E-08), (74182, 2.96623E-08), (74183, 1.60908E-08), (74184, 3.40070E-08), (74186, 3.12220E-08), (82206, 1.78732E-08), (82207, 1.78578E-08), (82208, 4.19446E-08), (83209, 7.82589E-08), (29063, 3.38912E-03), (29065, 1.51554E-03), (50112, 2.54666E-06), (50114, 1.73278E-06), (50115, 8.92643E-07), (50116, 3.81736E-05), (50117, 2.01632E-05), (50118, 6.35877E-05), (50119, 2.25524E-05), (50120, 8.55362E-05), (50122, 1.21557E-05), (50124, 1.52012E-05)

$Pb_{84.2}Li_{15.8}$
Density: 10172kgm^{-3}
(3006, 0.0948), (3007, 0.0632), (82204, 0.011788), (82206, 0.202922), (82207, 0.186082), (82208, 0.441208)

SS316
Atomic Density: 8.58301E-02barn^{-1}cm^{-1}
(26054, 3.29181E-03), (26056, 4.98289E-02), (26057, 1.13058E-03), (26058, 1.47865E-04), (6012, 1.19277E-04), (25055, 1.73653E-03), (14028, 7.86496E-04), (14029, 3.85593E-05), (14030, 2.45713E-05), (15031, 3.85117E-05), (16032, 1.41667E-05), (16033, 1.09980E-07), (16034, 6.02549E-07), (16036, 2.65303E-09), (24050, 7.46975E-04), (24052, 1.38506E-02), (24053, 1.54092E-03), (24054, 3.76464E-04), (28058, 7.00641E-03), (28060, 2.60890E-03), (28061, 1.11548E-04), (28062, 3.49927E-04), (28064, 8.63311E-05), (42092, 2.07981E-04), (42094, 1.26880E-04), (42095, 2.16071E-04), (42096, 2.24028E-04), (42097, 1.26943E-04), (42098, 3.17475E-04), (42100, 1.24166E-04), (7014, 2.71878E-04), (7015, 9.37261E-07), (5010, 9.50314E-07), (5011, 3.47739E-06), (29063, 1.57294E-04), (29065, 6.79509E-05), (27059, 4.04699E-05), (41093, 5.13489E-06), (22046, 8.56466E-06), (22047, 7.55943E-06), (22048, 7.33429E-05), (22049, 5.27248E-06), (22050, 4.94736E-06), (73181, 2.63837E-06)

H20
Density: 1000kgm^{-3}
(1001, 2.67614E-02), (1002, 1.53896E-06), (8016, 1.33497E-02)

Plasma
Atomic Density: 1x10^{-20} barn^{-1}cm^{-1}
(1002, 0.5), (1003, 0.5)

3 Scheme of Work Flowchart

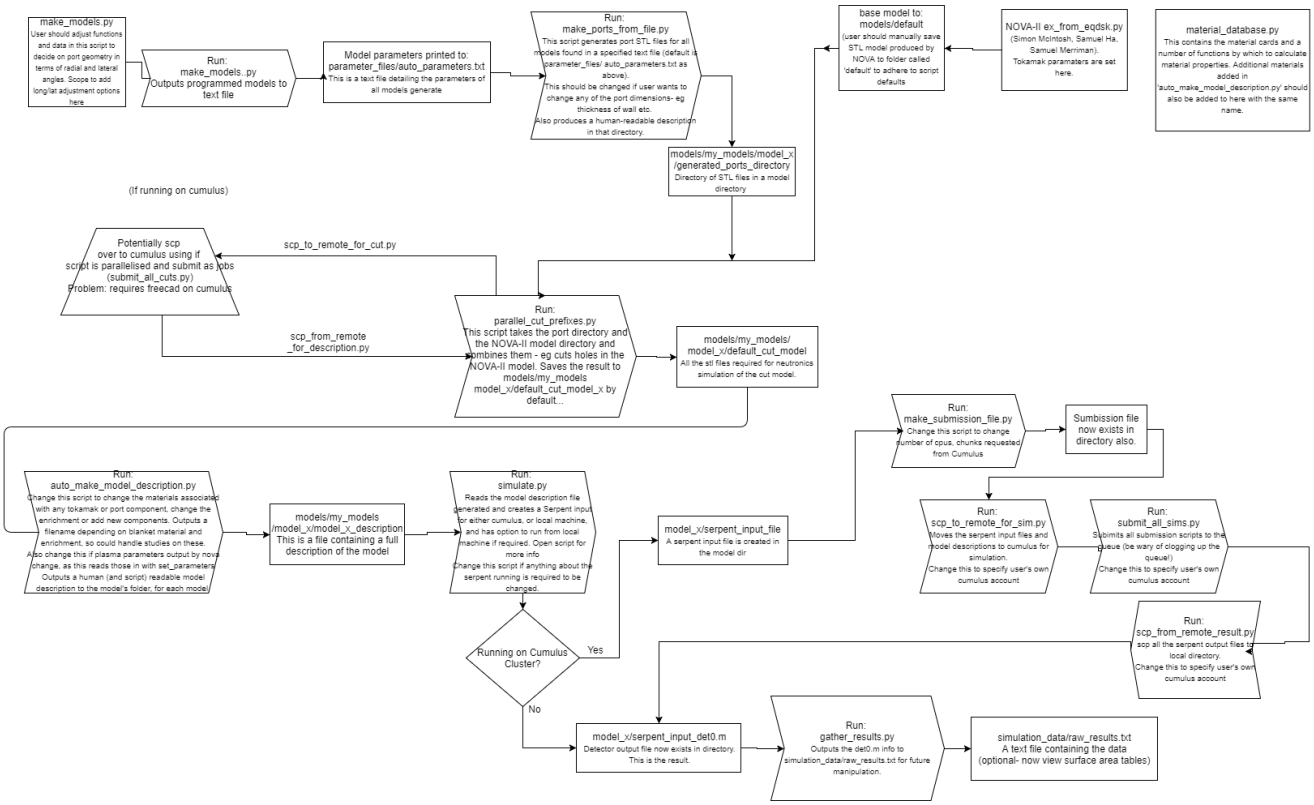

Fig a3.1: A flowchart of the scheme of work followed for scripting the experiment described in this report. This is the full process from the beginning to obtaining a TBR value for each model designed.

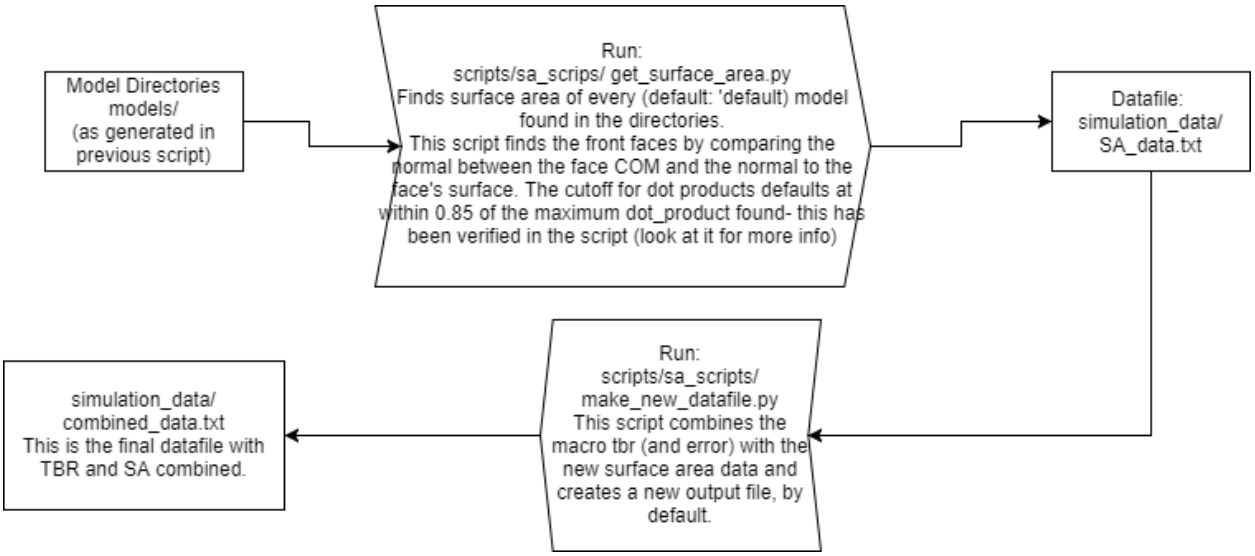

Fig a3.2: A flowchart of the scheme of work followed for finding a surface area for each model studied.